Reaction monitoring using SABRE-hyperpolarized benchtop (1 T) NMR spectroscopy

Olga Semenova,[a] Peter M. Richardson,[a] Andrew J. Parrott,[b] Alison Nordon,[b] Meghan E. Halse*[a] and Simon B. Duckett*[a]

a Centre for Hyperpolarisation in Magnetic Resonance, Chemistry, The University of York, York, YO10 5NY, UK.

b WestCHEM, Department of Pure and Applied Chemistry and CPACT, University of Strathclyde, Glasgow, G11XQ, UK

The conversion of [IrCl(COD)(IMes)] (COD = cis,cis-1,5-cyclooctadiene, IMes = 1,3-bis(2,4,6-trimethyl-phenyl)imidazole-2-ylidene) in the presence of an excess of *p*-H_2 and a substrate (4-aminopyridine (**4-AP**) or 4-methylpyridine (**4-MP**)) into $[Ir(H)_2(IMes)(substrate)_3]Cl$ is monitored by ^1H NMR spectroscopy using a benchtop (1 T) spectrometer in conjunction with the *para*hydrogen (*p*-H_2) based hyperpolarization technique signal amplification by reversible exchange (SABRE). A series of single-shot ^1H NMR measurements are used to monitor the chemical changes that take place in solution through the lifetime of the hyperpolarized response. Non-hyperpolarized high-field ^1H NMR control measurements were also undertaken to confirm that the observed time dependent changes relate directly to the underlying chemical evolution. The formation of $[Ir(H)_2(IMes)(substrate)_3]Cl$ is further linked to the hydrogen isotope exchange reaction (HIE) which leads to the incorporation of deuterium into the *ortho* positions of **4-AP**, where the source of deuterium is the solvent, methanol-d_4. Comparable reaction monitoring results are achieved at both high-field (9.4 T) and low-field (1 T). It is notable, that the low sensitivity of the benchtop (1 T) NMR enables the use of *protio* solvents, which is harnessed here to separate the effects of catalyst formation and substrate deuteration. Collectively, these methods illustrate how low-cost low-field NMR measurements provide unique insight into a complex catalytic process through a combination of hyperpolarization and relaxation data.

Introduction

Reaction monitoring using process analytical technology (PAT) is an important part of synthetic optimisation, reaction scale-up and industrial quality control.[1] While NMR spectroscopy is a well-established method for reaction monitoring, standard high-field (7 – 23 T) NMR spectrometers are large and costly to both purchase and operate thereby making them poorly suited to PAT applications. Recently, low-cost benchtop NMR spectrometers, based on permanent magnets with field strengths around 1 - 2 T, have become available.[2] These offer an opportunity to address the issue of cost whilst also providing a level of detector portability.[2] However, these instruments suffer from relatively low sensitivity and reduced chemical shift dispersion due to the lower magnetic field strengths which limits their viability for the study of low concentration analytes and nuclei with low NMR receptivity such as ^{13}C. One potential solution to this issue is to combine benchtop NMR with hyperpolarization.

Hyperpolarization is a term used to describe methods that generate NMR signal responses that are enhanced relative to those associated with nuclear spins at thermal equilibrium in the detection field.[3] Some of the most popular hyperpolarization methods today are dynamic nuclear polarization (DNP),[4] spin-exchange optical pumping (SEOP)[5] and *para*hydrogen induced polarization (PHIP).[6] In the context of industrial process monitoring, it is essential that the hyperpolarization process itself is low-cost and compact so that it does not compromise the advantages of benchtop NMR. Dissolution DNP has been integrated with benchtop NMR for monitoring the conversion of [1-^{13}C] pyruvate to [1- ^{13}C] lactate *in vitro* and *in vivo*.[7] However, the generation of hyperpolarized compounds by dissolution DNP is time consuming (ca. 90 mins per hyperpolarized sample), costly, and requires equipment with a large footprint. In contrast, we focus here on PHIP methods, which are relatively inexpensive and yield hyperpolarization in seconds.[8]

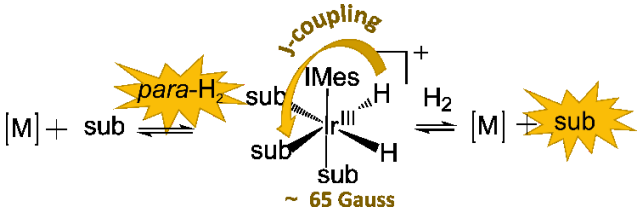

Figure 1. In the presence of an excess of *para*hydrogen and substrate, the exchange processes indicated enable polarization transfer from *p*-H_2 such that NMR resonances of the free substrate are enhanced. This transfer occurs most often a low magnetic field (0 – 200 G) through the scalar coupling network in the active complex and, due to reversibility, operates continuously when fresh *p*-H_2 is supplied.

In the traditional approach of Bowers and Weitekamp, parahydrogen induced polarization (PHIP) is achieved through hydrogenation of the molecule under investigation.[8a, 9] Introduced in 2009, the signal amplification by reversible exchange (SABRE) method is a non-hydrogenative version of PHIP that catalytically transfers *para*hydrogen (*p*-H_2) derived polarization without changing the chemical structure of the target compound.[10] In this technique *p*-H_2 and the target compound,

often called the substrate, bind reversibly to the metal centre of the SABRE catalyst (Figure 1). Once attached to the metal centre, the magnetic symmetry of p-H_2 is broken and the resultant hydride ligands are able to transfer their latent polarization into the bound substrate via the *J*-coupling network of the complex. This process can be optimised by using a weak magnetic field that often lies in the range of 0 - 200 G depending on the type of nucleus that is to receive the polarization.[11] The SABRE method is reversible, taking seconds to build up polarisation while target molecules can be re-polarized by adding fresh p-H_2. Therefore, it provides a fast and renewable or indeed continuous route to hyperpolarization. Due to relatively cheap methods for generating and storing p-H_2, and the comparative simplicity of the SABRE method, this is an attractive approach for industrial process monitoring using hyperpolarized benchtop NMR.[8] Indeed, SABRE has already been combined with benchtop NMR to enhance ^{1}H, ^{13}C and ^{15}N NMR signals.[12] One of the limitations of the SABRE method compared to other approaches such as DNP is the range of substrates that are amenable to hyperpolarization, with the best results being observed for N-heterocycles. However, many groups are working to expand the scope of the SABRE method in order to make it more generally applicable.[12d, 13] Additionally a number of articles have proposed routes to achieve biocompatible SABRE hyperpolarization with a view to *in vivo* detection of biomolecules.[14]

In this work, we introduce a method to follow reactivity using single-shot measurements that probe both the lifetime and the magnitude of a SABRE-enhanced ^{1}H NMR response. Such measurements can be easily completed at either high- or low-field. To illustrate this method and its benefits, we follow the reaction in which the SABRE pre-catalyst converts into the active catalyst. Specifically, we monitor the formation of $[Ir(H)_2(IMes)(substrate)_3]Cl$ (IMes = 1,3-bis(2,4,6-trimethylphenyl)imidazole-2-ylidene).[15] Because iridium complexes facilitate the hydrogen isotope exchange (HIE) reaction, deuteration of the substrate is observed during this process in methanol-d_4.[10, 16] High-field (9.4 T, 400 MHz) ^{1}H NMR detection is initially used to measure the changes in SABRE hyperpolarization lifetimes during the catalyst activation and HIE reactions. Parallel non-hyperpolarized ^{1}H NMR measurements are completed to link the observed changes in hyperpolarization lifetime to the underlying chemical changes in solution. Due to reduced sensitivity and increased peak overlap in ^{1}H NMR spectra acquired at 1 T (43 MHz), standard ^{1}H NMR reaction monitoring of these processes cannot be achieved using benchtop NMR. We overcome these limitations by using our hyperpolarized response whilst also exploiting the inherent low sensitivity of a benchtop NMR spectrometer to allow experiments in non-deuterated solvents to fully differentiate the effects of the active SABRE catalyst formation from target substrate deuteration.

Experimental

Sample preparation

NMR samples were prepared from a 0.6 mL solution of 5 mM [IrCl(COD)(IMes)] (COD = cis,cis-1,5-cyclooctadiene, IMes = 1,3-bis(2,4,6-trimethyl-phenyl)imidazole-2-ylidene) in methanol-d_4 or *protio* methanol by adding 15 µmol **4-AP** or **4-MP** (5 equivalents with respect to the SABRE pre-catalyst **1**) in a 5 mm NMR tube fitted with a Young's tap (GPE Scientific Ltd, Leighton Buzzard, UK). The samples were degassed using a three-stage freeze-pump-thaw method in a bath of dry-ice and acetone. The pre-catalyst was synthesized in-house and the **4-AP** and **4-MP** were purchased from Sigma Aldrich (Sigma-Aldrich Company Ltd., Gillingham, UK) and used without further modification. ^{1}H, ^{13}C and ^{15}N NMR characterisation data for **4-AP**, **4-MP**, [Ir(COD)(IMes)(substrate)]Cl and $[Ir(H)_2(IMes)(substrate)_3]Cl$ (substrate = **4-AP** or **4-MP**) is available in the supporting information.

SABRE catalyst activation monitoring using standard ^{1}H NMR

Solutions containing the pre-catalyst **1** with either **4-AP** or **4-MP** in methanol-d_4 or *protio* methanol formed the unactivated catalyst [Ir(COD)(IMes)(substrate)]Cl. 0.6 mL of this initial solution was added to a 5 mm NMR tube equipped with a Young's tap and degassed following the sample preparation procedure described above. When **4-MP** was used as the substrate, peaks corresponding to the pre-catalyst **1** were observed in the prepared solution and were quantified by ^{1}H NMR at 400 MHz as contributing 15% of the signal, suggesting 85% of **1** had converted to the unactivated catalyst [Ir(COD)(IMes)(**4-MP**)]Cl at equilibrium. In contrast, no ^{1}H NMR peaks corresponding to **1** were observed in the initial ^{1}H NMR spectra for samples where **4-AP** was used as the substrate, suggesting full conversion to **2**. When the conversion of pre-catalyst **1** into [Ir(COD)(IMes)(**4-AP**)]Cl **2** was monitored by ^{1}H NMR spectroscopy for a sample containing 5 mM of **1** and **25** mM of **4-AP** in methanol-d_4 at 280 K, the reaction took 14 minutes to reach completion.

To monitor the formation of the active complex $[Ir(H)_2(IMes)(substrate)_3]Cl$ (substrate = **4-AP** or **4-MP**), H_2 (4 bar absolute) was added to the headspace of the NMR tube. The sample was shaken vigorously for around 5 s and inserted into the NMR spectrometer (Bruker AVIII 400 MHz) at 298 K. A series of ^{1}H spectra was acquired over a period of 15.5 hours (Figure S4, Supporting Information).

Measurement of hyperpolarized signal

SABRE hyperpolarization transfer experiments were performed under 4 bar p-H_2 that was produced by cooling H_2 gas over a paramagnetic catalyst[8b, 17] at 28 K to yield >99% *para*-enrichment. After the *para*-enriched H_2 was added to the headspace of the NMR tube, the sample was shaken for 5 s in a polarization transfer field (PTF) of 6.1 ± 0.3 mT (61 ± 3 G) generated by a hand-held magnet array,[12c] to dissolve the p-H_2 into solution and allow for polarization transfer to occur. Immediately following shaking, the sample was transferred manually into the spectrometer for a single-shot NMR measurement using either a single 90° radio frequency (RF) pulse followed by acquisition of the FID or a variable flip angle single-shot T_1 sequence (details below). ^{1}H NMR spectra were acquired on either a Bruker AVIII 400 MHz spectrometer (9.4 T) or a Magritek Spinsolve Carbon 43 MHz benchtop NMR spectrometer (1 T). Between each hyperpolarization measurement, the headspace of the NMR tube was refreshed with p-H_2 via the diffusion between the NMR tube headspace and a line filled with fresh p-H_2. The sample was left to equilibrate for 10 s and the procedure was repeated twice. This non-aggressive way of refreshing p-H_2 was employed to reduce solvent evaporation and thereby maintain relative catalyst and substrate concentrations throughout.

Hyperpolarized single-shot T_1 measurement

The single-shot hyperpolarized T_1 measurements were achieved by acquiring a series of 15 ^{1}H NMR spectra, where the excitation pulse for each acquisition was achieved using RF pulses of increasing flip angle (see the SI for more details). The variable flip angles were chosen to excite an equal fraction of the available magnetization at each step of the experiment in order to simplify the T_1 analysis and optimise the signal-to-noise ratio. The variable time delays between acquisitions were chosen to ensure full coverage of the T_1 decay curve. To remove the influence of thermally- polarized background ^{1}H NMR signals from the T_1 analysis, a reference scan was acquired after each hyperpolarized T_1 measurement. This was achieved by holding the sample outside of the NMR spectrometer for 1-1.5 minutes to ensure full relaxation of all polarization and then manually inserting the sample into the NMR spectrometer and carrying out a single-shot T_1 experiment. The resultant thermally-polarized NMR spectra were integrated and subtracted from the hyperpolarized signals prior to T_1 analysis. Hyperpolarized relaxation times (T_1) were determined from an exponential fit of the corrected hyperpolarized signal decay according to equation 1, where $M(t)$ is magnetization, M_0 is the initial magnetization, T_1 is the time constant, t is the time since the application of the first RF pulse, M_{offset} is the offset magnetization.

$$M(t) = M_0 e^{\left(-t/T_1\right)} + M_{offset} \qquad (1)$$

Full details on the variable flip angle pulse sequence and the parameters used are available in the supporting information.

Results

Reactivity of [Ir(COD)(IMes)(4-AP)]Cl with H_2 and 4-AP in MeOD

In order to prepare a SABRE active catalyst, 5 mM of the pre-catalyst with the general formula [Ir(Cl)(COD)(NHC)], where NHC is an N-heterocyclic carbene (complex **1** in Figure 2a), is mixed with an excess of the substrate. In this study we used the substrate 4-aminopyridine (**4-AP**), a potassium channel blocker known as dalfampridine, that is registered as a drug for walking improvement in patients with multiple sclerosis.[18] Once this substrate was added to the pre-catalyst, the chloride ion is displaced to form complex **2** (Figure 2a). When hydrogen gas was added to the resulting solution, complex **2** first oxidatively adds H_2 to form the octahedral dihydride complex **3**. The cyclooctadiene ligand in this complex was then hydrogenated to ultimately form cyclooctane (COA), which can no longer ligate. Consequently, the activated SABRE complex **4** was then formed in solution with three ligated molecules of **4-AP** and two hydrides as shown in Figure 2a.[19] When monitored by ^{1}H NMR spectroscopy at room temperature, no peaks for complex **1** were detected at 6 minutes (first scan). However, the transformation from **2** to **4** can be monitored through their unique NHC proton resonances at 7.32 ppm (complex **2**, cyan squares) and 6.96 ppm (complex **4**, teal squares).

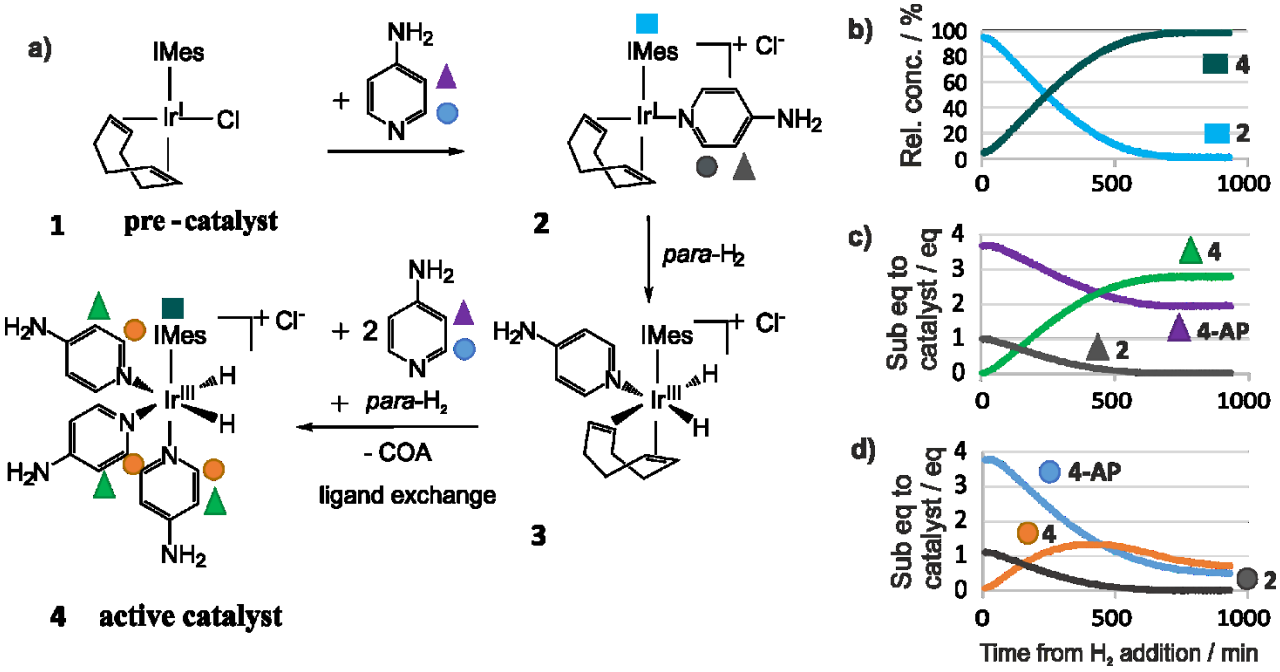

Figure 2. (a) Mechanism for the conversion of **1** to **4** in the presence of **4-AP** and H_2. First **1** transforms into [Ir(COD)(IMes)(**4-AP**)]Cl (**2**) which then adds H_2 to form the octahedral dihydride complex [Ir(H)$_2$(COD)(IMes)(**4-AP**)]Cl (**3**) which is not stable at room temperature. COD hydrogenation then follows and **3** converts to [Ir(H)$_2$(IMes)(**4-AP**)$_3$]Cl (**4**) by binding two more molecules of **4-AP**. (b-d) Time dependent relative signal intensities calculated from a series of ^{1}H NMR spectra acquired over the course of the reaction at 298 K for a sample under a 4 bar pressure of H_2 where the initial concentrations of **1** and **4-AP** are 5 mM and 25 mM respectively. H_2 was added and the sample shaken only once at the start of the experiment. (b) Evolution of the carbene ligand signals of **2** (square cyan) and **4** (square teal), (c) Evolution of the *meta* proton resonance of free and bound **4-AP** (purple, grey and green triangles) and (d) Evolution of the *ortho* proton resonance of free and bound **4-AP** (blue, grey and orange circles).

This conversion can also be monitored via the *ortho* and *meta* proton resonances of **4-AP** in complex **2** (grey circles and triangles), complex **4** (orange circles and green triangles) and in free solution (blue circles and purple triangles). Figure 2 presents the results of ^{1}H NMR monitoring of the SABRE catalyst activation process over a period of 15.5 hours at room temperature. Figure 3 shows four representative NMR spectra obtained during the monitoring period. As illustrated in Figure 2b, full conversion of **2** (cyan squares) to **4** (teal squares) occurs after approximately 11 hours. Compared to other studies,[14b, 20] the formation of **4** from **2** with **4-AP** is very slow. This is a reflection of the rate of addition of H_2 to **2**. By contrast, as described later in this paper, for the case of **4-MP**, the formation of [Ir(H)$_2$(IMes)(**4-MP**)$_3$]Cl is much faster (Figures S4, SI). This suggests that intermediate dihydride complex forms much more rapidly when **4-MP** is the substrate. Monitoring of the *meta* resonances of **4-AP** (Figure 2c) confirms this conversion from **2** (grey triangles) to **4** (green triangles) while also demonstrating the consumption of two equivalents of **4-AP** in free solution (purple triangles), as expected. In contrast, the *ortho* proton resonances of **4-AP** show a different dependence on time (Figure 2d). The intensity of the *ortho* resonance of **4-AP** in complex **4** increases initially, as expected, but decays at longer times. Similarly, the intensity of the *ortho* resonance of **4-AP** in solution decays initially as expected but continues to reduce even after the formation of **4** is complete. These observations are consistent with the deuteration of the *ortho* positions of **4-AP** (Scheme 1), where the source of deuterium is the methanol-d_4, used as the solvent. These results suggest that deuteration happens on the same timescale as catalyst activation and an analysis of the relative intensities of the *ortho* and *meta* resonances of **4-AP** indicate that the *ortho* position deuteration level reaches 75% by the end of the experiment (15.5 h). Further evidence for this *ortho* position deuteration was evident in the appearance of the corresponding ^{1}H NMR spectra, where there were significant changes in the line-shape of the *meta* resonances of **4-AP** (Figure S1, SI). No deuteration of the *meta* positions was observed on the timescale of the experiment. Additional details and example spectra are provided in the supporting information.

Scheme 1. Deuteration of *ortho* positions of 4-aminopyridine in the presence of iridium complexes **3** and **4** and H_2 in methanol-d_4.

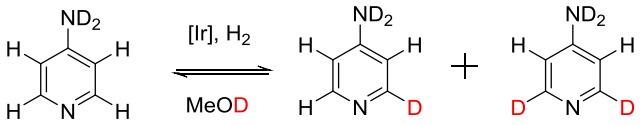

Reaction monitoring with SABRE

We seek to establish here that the SABRE-enhanced NMR response can be assessed through either the amplitude or the lifetime of the SABRE hyperpolarization. Both of these parameters have the potential to act as probes for reaction monitoring and require the collection of data at a series of reaction time points. The SABRE-lifetime measurements are themselves collected through a series of single-shot acquisitions that can be repeated on the timescale of five T_1 periods which means that a typical observation time reflects a couple of minutes.[10, 21] The amplitude of the SABRE signal is expected

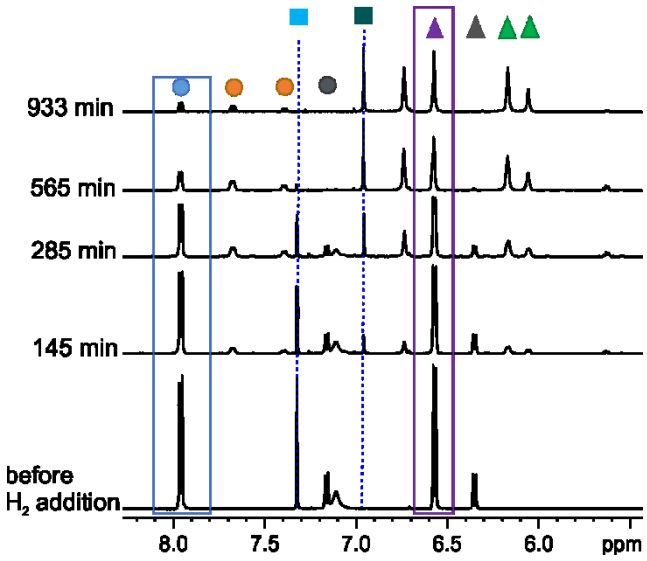

Figure 3. ^{1}H NMR spectra recorded at 9.4 T associated with the data in Figure 2 at the indicated time points with analogous color-coding to demonstrate speciation changes. It is noteworthy that the splitting on the *meta* signal for **4-AP** (6.57 ppm) evolves into a singlet due to the deuteration of the *ortho* site (7.96 ppm) over the course of the reaction. The signals of interest are surrounded by the colored boxes. The dashed lines correspond with the carbene signals in catalysts **2** and **4**.

to provide information on the activation process because the degree of signal amplification will increase as the concentration of active catalyst **4** increases. However, the effect of substrate deuteration on this signal is expected to be complicated. Previous work by Rayner *et al.* has suggested that deuteration can lead to increased SABRE efficiency due to a lengthening of the lifetimes of the remaining ^{1}H resonances within the substrate, and the concentration of the SABRE hyperpolarization into fewer nuclei.[22] However, there is also potential for deuteration to decrease SABRE polarization transfer efficiency through changes to the *J*-coupling network that drives polarization transfer in the low-field regime.[11a, 11b, 22-23] Observations of the changes in the SABRE-enhanced ^{1}H NMR signal intensity with time suggest that this parameter is sensitive to both of the chemical transformations under investigation (Figure S5, SI). However, the interpretation of these effects is complicated by the fact that the SABRE response is not linearly dependent on substrate concentration in this case. In addition, any quantitative interpretation would be limited by the reproducibility of the SABRE response, which depends on many factors including *p*-H_2 enrichment level, polarization transfer field, polarization build-up time, and sample transport time. Therefore, we focus here on the use of the lifetime of the SABRE hyperpolarization to monitor reactivity.

The lifetime of the SABRE hyperpolarization is limited by longitudinal (T_1) NMR relaxation times, which are sensitive to the chemical environment and have been widely used for identifying and characterising inter- and intramolecular interactions.[24] In this method, we exploit the fact that in the presence of the active SABRE catalyst, the substrate molecules in free solution and those bound to **4** are in rapid chemical exchange. As a result, the observed lifetime of the SABRE hyperpolari-

zation reflects a weighted average of the lifetime for substrate molecules bound to **4** and substrate molecules in free solution.[25] NMR relaxation times are known to be significantly shorter for the bound substrate molecules.[25] Therefore, as the concentration of the active SABRE catalyst **4** increases, the observed hyperpolarization lifetime is expected to decrease. This shortening of the relaxation times in the presence of the activated complex is a well-known effect in the SABRE literature.[22, 25] In addition, the observed lifetime of the SABRE hyperpolarization of the *meta* resonances of **4-AP** is expected to increase following substitution of ^{2}H for ^{1}H in the adjacent *ortho* position (Scheme 1).[22, 26] Therefore the time-dependent changes of the hyperpolarization lifetimes for the *meta* resonances of **4-AP** are expected to reflect the competing effects of the formation of **4** and the partial deuteration of **4-AP**. In contrast, the hyperpolarization lifetimes for the *ortho* resonances of **4-AP** are expected to reflect only the formation of **4**. This is because a ^{1}H NMR signal will only be observed for the ^{1}H *ortho* resonances of 4-aminopyridine and 4-amino-2-d_1-pyridine. In both of these cases, the observed *ortho* ^{1}H hyperpolarization lifetime will be dominated by interactions with the ^{1}H in the adjacent *meta* position and therefore is not expected to be affected significantly by the progress of the ^{1}H - ^{2}H exchange reaction.[22]

Parallel measurements of non-hyperpolarized ^{1}H NMR spectra and hyperpolarization lifetimes were performed as a function of time following the first addition of *p*-H_2 with detection on a 400 MHz NMR spectrometer in methanol-d_4 (Figure 4a and b). Non-hyperpolarized ^{1}H NMR spectra indicate that the formation of **4** is complete by 230 min following the first addition of *p*-H_2 (Figure 4a). This activation time is indicated by the vertical dashed lines in Figure 4b-d. Figure 4b shows the change in the *ortho* (blue circles) and *meta* (purple triangles) ^{1}H hyperpolarization lifetimes as a function of time following the initial addition of *p*-H_2. Each hyperpolarization lifetime measurement is achieved using a manual shaking SABRE procedure with NMR detection at 9.4 T and where the *p*-H_2 in the headspace of the NMR tube was refreshed between each measurement. In Figure 4b, the hyperpolarization lifetimes for the *ortho* resonances of **4-AP** reduce and reach a plateau in a time period that corresponds to the formation of **4**. In contrast, the lifetimes of the *meta* resonances show an initial rapid increase with a subsequent decrease at longer times. These observations support our hypothesis that the hyperpolarization lifetimes of the *meta* resonances are sensitive to both the formation of **4** and substrate deuteration, while the hyperpolarization lifetimes of the *ortho* resonances are sensitive only to the formation of **4**. The initial change in the lifetime of the *meta* resonances indicate a more rapid incorporation of ^{2}H into **4-AP** when *p*-H_2 was replenished between measurements rather than added once at the start of the experiment (Figure 2). This increase in the rate of the HIE reaction is supported the observed changes in the lineshape of the *meta* resonances in the standard ^{1}H NMR spectra acquired at 400 MHz (Figure S3, SI).

The use of SABRE hyperpolarization to increase sensitivity allows us to repeat this reaction monitoring procedure on a 1 T benchtop NMR spectrometer (Figure 4c). The time-dependent changes in hyperpolarization lifetime determined using the benchtop NMR instrument show the same trends as the experiments using a standard (9.4 T) NMR spectrometer. This illustrates that SABRE hyperpolarization can be used to enable reaction monitoring at both high and low field. In fact, here we use benchtop NMR where a combination of low sensitivity and peak overlap would normally prevent this monitoring process. Furthermore, once the sensitivity limitation is overcome through the use of hyperpolarization, there are additional benefits to using benchtop NMR. Due to its lower magnetic field strength, benchtop ^{1}H NMR spectra can be acquired in the presence of a protonated solvent without the need to actively suppress the solvent signal. Indeed it has been found that the SABRE hyperpolarized NMR response from a low-concentration analyte can exceed that from a protonated solvent when detected at 1 T (43 MHz).[12b] Figure 4d shows the change in the *ortho* (blue circles) and *meta* (purple triangles) ^{1}H hyperpolarization lifetimes as a function of time following the initial addition of *p*-H_2 for the case where *protio* methanol is the solvent and a 1 T benchtop NMR spectrometer is used for detection. In the absence of the source of deuterium (methanol-d_4) the hyperpolarization lifetimes of both the *ortho* and *meta* protons follow the same trend: a monotonic decrease to a plateau on the same timescale as the formation of the activated SABRE complex, **4**. The absence of the initial increase in the *meta* hyperpolarization lifetime supports the hypothesis that

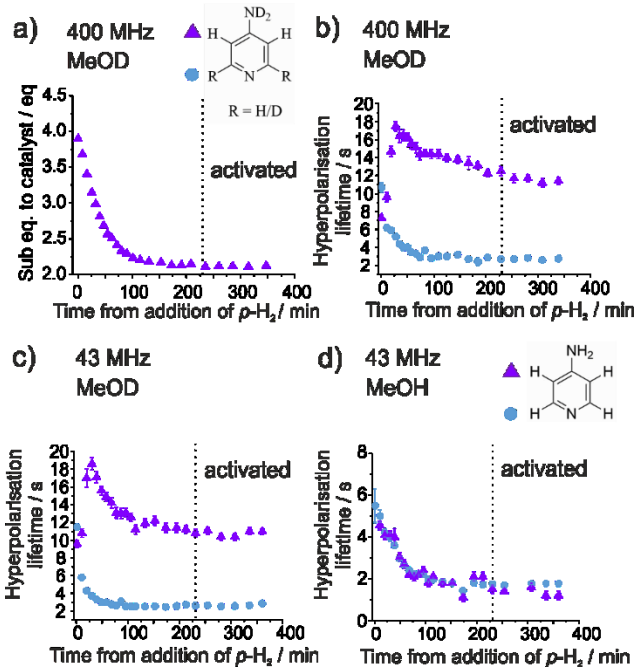

Figure 4. (a) Non-hyperpolarized ^{1}H NMR signal integrals of the **4-AP** *meta* proton resonance, acquired in parallel with the hyperpolarization lifetime measurements of (b) at 400 MHz in methanol-d_4. (b) Hyperpolarization signal lifetimes of the *ortho* (blue circles) and *meta* (purple triangles) proton resonances of **4-AP** as a function of time after H_2 addition in methanol-d_4 at 9.4 T, (c) as (b) but recorded at 1 T, and (d) as (c) but in *protio* methanol. The initial concentration of **4-AP** is 25 mM, which gives a 2-fold excess relative to [Ir(H)$_2$(IMes)(**4-AP**)$_3$]Cl (5 mM) once its formation is complete. Error bars indicate the standard error from the fit to the hyperpolarization decay curve specified by Equation 1. The time point for complete conversion to **4** is represented by the vertical line.

this feature of the previous experiments originated from the deuteration effect. Therefore not only does the use of SABRE hyperpolarization enable reaction monitoring using a benchtop NMR spectrometer, the use of this low-field (1 T) instrument provides a simple route to the deconvolution of the competing effects of SABRE catalyst activation and substrate deuteration.

To further verify the method, we have applied it to an analogous SABRE system where the substrate is 4-methylpyridine (**4-MP**). When the reaction is monitored after a single exposure to H_2, even though rapid formation of $[Ir(H)_2(IMes)(\mathbf{4\text{-}MP})_3]Cl$ (~ 50 min) is indicated, the timescale for deuteration is comparable to that with **4-AP**. This suggests that $[Ir(H)_2(IMes)(\mathbf{4\text{-}AP})_3]Cl$ is more active for the HIE reaction than $[Ir(H)_2(IMes)(\mathbf{4\text{-}MP})_3]Cl$ (Figures S4, SI). This difference in behavior is consistent with the predicted C-H bond strengths in the substrates on the basis of inductive changes. One further consequence of this behavior is that when the hyperpolarized lifetimes are probed over the first 65 minutes, rapid catalyst activation is observed with negligible deuteration. The analogous hyperpolarized lifetimes in protonated methanol exhibit the same trend, further supporting the deduction of the absence of significant deuteration on the timescale of the experiment (Figures S9 and S10, SI).

Conclusions

We have introduced a method for using SABRE-enhanced ^{1}H NMR spectroscopy to monitor reactivity, even at a mM concentration level, through the quantification of hyperpolarization lifetimes. This method was used to monitor the formation of the active SABRE catalyst from a pre-catalyst and hydrogen isotope exchange within the substrate, 4-aminopyridine. This method was demonstrated using both high-field (9.4 T, 400 MHz) and benchtop (1 T, 43 MHz) NMR detection. Comparable results were obtained at both fields, illustrating the utility of this approach for reaction monitoring on a benchtop NMR spectrometer even under conditions where thermal ^{1}H NMR cannot be used due to low sensitivity and peak overlap. In addition, the use of a low-field benchtop NMR spectrometer for detection allowed experiments to be carried out in a *protio* solvent. For the reactivity explored herein, this provided a route to separating out the effects of the formation of the SABRE catalyst and the hydrogen isotope exchange reaction, by removing the source of ^{2}H for the isotope exchange, methanol-d_4. More generally, the ability to carry out reaction monitoring in a non-deuterated solvent renders this method more attractive for industrial applications where metal complexes are used to achieve high value organic transformations, as it removes the need for costly sample preparation step prior to analysis.[27]

The studies completed in this work followed reactivity under two different regimes within a sealed NMR tube. First in the absence of stirring where slow diffusion of hydrogen across the gas-liquid interface is expected. Second, where hydrogen in solution was replenished between experiments through vigorous shaking of the NMR tube. In future work, a flow-based SABRE approach, where p-H_2 is bubbled through the solution outside of the spectrometer,[28] could provide a route to automating the reaction monitoring method and providing more control over the reaction conditions.

In situ SABRE measurements, where detection is achieved in mT-μT magnetic fields such as the Earth's magnetic field, could also be used to provide increased control over the reaction conditions throughout the monitoring process. However, in this case there would be a need for reference measurements to isolate the source of the hyperpolarized response as no chemical shift information is available in such ultra-low-field NMR spectra. The quantitative aspects of the method can be improved by calibrating the hyperpolarization lifetimes to link changes in lifetime to changes in the concentration of the active SABRE species.

ASSOCIATED CONTENT

Supporting Information

The Supporting Information is available free of charge on the ACS Publications website.

Additional information as noted in text (PDF)

AUTHOR INFORMATION

Corresponding Author

* Meghan Halse meghan.halse@york.ac.uk
* Simon Duckett simon.duckett@york.ac.uk

Notes

The authors declare no competing financial interest.

ACKNOWLEDGMENT

The authors would like to thank Dr Richard John for NMR support, Dr Victoria Annis for synthesis of the SABRE catalyst and the EPSRC (EP/M020983/1) and Wellcome Trust (092506 and 098335) for funding. OS would like to thank Pfizer, Department of Chemistry Wild Fund Scholarship and the University of York for PhD studentship funding.

REFERENCES

1. (a) Bakeev, K. A., In Process analytical technology : spectroscopic tools and implementation strategies for the chemical and pharmaceutical industries, Bakeev, K. A., Ed. Blackwell Publishing Ltd: Oxford, 2005; pp 13-39; (b) Rathore, A. S.; Bhambure, R.; Ghare, V., Process analytical technology (PAT) for biopharmaceutical products. Anal. Bioanal. Chem. **2010,** 398 (1), 137-154.
2. (a) Foley, D. A.; Zeil, M. T.; Marquez, B. L.; Kaerner, A., NMR Reaction-Monitoring as a Process Analytical Technique. Pharm. Technol. **2011,** 2011 Supplement (6), 19-21; (b) Sans, V.; Porwol, L.; Dragone, V.; Cronin, L., A self optimizing synthetic organic reactor system using real-time in-line NMR spectroscopy. Chem. Sci. **2015,** 6 (2), 1258-1264; (c) Musio, B.; Gala, E.; Ley, S. V., Real-Time Spectroscopic Analysis Enabling Quantitative and Safe Consumption of Fluoroform during Nucleophilic Trifluoromethylation in Flow. ACS Sustainable Chem. Eng. **2018,** 6 (1), 1489-1495; (d) Singh, K.; Danieli, E.; Blümich, B., Desktop NMR spectroscopy for real-time monitoring of an acetalization reaction in comparison with gas chromatography and NMR at 9.4 T. Anal. Bioanal. Chem. **2017,** 409 (30), 7223-7234; (e) Schumacher, S. U.; Rothenhäusler, B.; Willmann, A.; Thun, J.; Moog, R.; Kuentz, M., Time domain NMR as a new process monitoring method for characterization of pharmaceutical hydrates. J. Pharm. Biomed. Anal. **2017,** 137, 96-103; (f) Blümich, B., Introduction to compact NMR: A review of methods. TrAC Trends in Analytical Chemistry **2016,** 83, 2-11; (g) Meyer, K.; Kern, S.; Zientek, N.; Guthausen, G.; Maiwald, M., Process control with compact NMR. TrAC Trends in Analytical Chemistry **2016,** 83, 39-52; (h) Singh, K.; Blümich, B., NMR spectroscopy with compact instruments. TrAC Trends in Analytical Chemistry **2016,** 83, 12-26.

3. (a) Halse, M. E., Perspectives for hyperpolarisation in compact NMR. Trac-Trends in Analytical Chemistry **2016,** 83, 76-83; (b) Ardenkjaer- Larsen, J. H.; Boebinger Gregory, S.; Comment, A.; Duckett, S.; Edison Arthur, S.; Engelke, F.; Griesinger, C.; Griffin Robert, G.; Hilty, C.; Maeda, H.; Parigi, G.; Prisner, T.; Ravera, E.; van Bentum, J.; Vega, S.; Webb, A.; Luchinat, C.; Schwalbe, H.; Frydman, L., Facing and Overcoming Sensitivity Challenges in Biomolecular NMR Spectroscopy. Angewandte Chemie International Edition **2015,** 54 (32), 9162-9185.

4. Ardenkjaer-Larsen, J. H., On the present and future of dissolution-DNP. J. Magn. Reson. **2016,** 264, 3-12.

5. (a) Berthault, P.; Huber, G.; Desvaux, H., Biosensing using laser-polarized xenon NMR/MRI. Prog. Nucl. Magn. Reson. Spectrosc. **2009,** 55 (1), 35-60; (b) Walker, T. G.; Happer, W., Spin-exchange optical pumping of noble-gas nuclei. Rev. Mod. Phys. **1997,** 69 (2), 629-642.

6. (a) Duckett, S. B.; Mewis, R. E., Application of Parahydrogen Induced Polarization Techniques in NMR Spectroscopy and Imaging. Accounts of Chemical Research **2012,** 45 (8), 1247-1257; (b) Hovener, J.; Pravdivtsev Andrey, N.; Kidd, B.; Bowers, C. R.; Glöggler, S.; Kovtunov Kirill, V.; Plaumann, M.; Katz-Brull, R.; Buckenmaier, K.; Jerschow, A.; Reineri, F.; Theis, T.; Shchepin Roman, V.; Wagner, S.; Zacharias Niki, M. M.; Bhattacharya, P.; Chekmenev Eduard, Y., Parahydrogen- based Hyperpolarization for Biomedicine. Angewandte Chemie International Edition **2018,** 0 (ja).

7. (a) Tee, S. S.; DiGialleonardo, V.; Eskandari, R.; Jeong, S.; Granlund, K. L.; Miloushev, V.; Poot, A. J.; Truong, S.; Alvarez, J. A.; Aldeborgh, H. N.; Keshari, K. R., Sampling Hyperpolarized Molecules Utilizing a 1 Tesla Permanent Magnetic Field. Scientific Reports **2016,** 6, 32846; (b) Hirsch, M. L.; Kalechofsky, N.; Belzer, A.; Rosay, M.; Kempf, J. G., Brute-Force Hyperpolarization for NMR and MRI. J. Am. Chem. Soc. **2015,** 137 (26), 8428-8434.

8. (a) Duckett, S. B.; Sleigh, C. J., Applications of the parahydrogen phenomenon: A chemical perspective. Prog. Nucl. Magn. Reson. Spectrosc. **1999,** 34 (1), 71-92; (b) Natterer, J.; Bargon, J., Parahydrogen induced polarization. Prog. Nucl. Magn. Reson. Spectrosc. **1997,** 31 (4), 293-315.

9. Bowers, C. R.; Weitekamp, D. P., Transformation of Symmetrization Order to Nuclear-Spin Magnetization by Chemical Reaction and Nuclear Magnetic Resonance. Phys. Rev. Lett. **1986,** 57 (21), 2645-2648.

10. Adams, R. W.; Aguilar, J. A.; Atkinson, K. D.; Cowley, M. J.; Elliott, P. I. P.; Duckett, S. B.; Green, G. G. R.; Khazal, I. G.; López-Serrano, J.; Williamson, D. C., Reversible Interactions with para-Hydrogen Enhance NMR Sensitivity by Polarization Transfer. Science **2009,** 323 (5922), 1708.

11. (a) Theis, T.; Truong, M. L.; Coffey, A. M.; Shchepin, R. V.; Waddell, K. W.; Shi, F.; Goodson, B. M.; Warren, W. S.; Chekmenev, E. Y., Microtesla SABRE enables 10% nitrogen-15 nuclear spin polarization. J. Am. Chem. Soc. **2015,** 137 (4), 1404-1407; (b) Ivanov, K. L.; Pravdivtsev, A. N.; Yurkovskaya, A. V.; Vieth, H.-M.; Kaptein, R., The role of level anti-crossings in nuclear spin hyperpolarization. Prog. Nucl. Magn. Reson. Spectrosc. **2014,** 81, 1-36; (c) Adams, R. W.; Duckett, S. B.; Green, R. A.; Williamson, D. C.; Green, G. G. R., A theoretical basis for spontaneous polarization transfer in non-hydrogenative parahydrogen-induced polarization. J. Chem. Phys. **2009,** 131 (19), 194505.

12. (a) Colell, J. F. P.; Emondts, M.; Logan, A. W. J.; Shen, K.; Bae, J.; Shchepin, R. V.; Ortiz, G. X.; Spannring, P.; Wang, Q.; Malcolmson, S. J.; Chekmenev, E. Y.; Feiters, M. C.; Rutjes, F. P. J. T.; Blümich, B.; Theis, T.; Warren, W. S., Direct Hyperpolarization of Nitrogen-15 in Aqueous Media with Parahydrogen in Reversible Exchange. J. Am. Chem. Soc. **2017,** 139 (23), 7761-7767; (b) Richardson, P. M.; Parrott, A. J.; Semenova, O.; Nordon, A.; Duckett, S. B.; Halse, M. E., SABRE hyperpolarization enables high-sensitivity 1H and 13C benchtop NMR spectroscopy. Analyst **2018,** 143 (14), 3442-3450; (c) Richardson, P. M.; Jackson, S.; Parrott, A. J.; Nordon, A.; Duckett, S. B.; Halse, M. E., A simple hand-held magnet array for efficient and reproducible SABRE hyperpolarisation using manual sample shaking. Magnetic Resonance in Chemistry **2017,** 56 (7), 641-650; (d) Lehmkuhl, S.; Wiese, M.; Schubert, L.; Held, M.; Küppers, M.; Wessling, M.; Blümich, B., Continuous hyperpolarization with parahydrogen in a membrane reactor. J. Magn. Reson. **2018,** 291, 8-13.

13. (a) Iali, W.; Rayner, P. J.; Duckett, S. B., Using parahydrogen to hyperpolarize amines, amides, carboxylic acids, alcohols, phosphates, and carbonates. Science Advances **2018,** 4 (1), eaao6250; (b) Logan, A. W. J.; Theis, T.; Colell, J. F. P.; Warren, W. S.; Malcolmson, S. J., Hyperpolarization of Nitrogen-15 Schiff Bases by Reversible Exchange Catalysis with para-Hydrogen. Chemistry **2016,** 22 (31), 10777-10781; (c) Zeng, H.; Xu, J.; Gillen, J.; McMahon, M. T.; Artemov, D.; Tyburn, J.-M.; Lohman, J. A. B.; Mewis, R. E.; Atkinson, K. D.; Green, G. G. R.; Duckett, S. B.; van Zijl, P. C. M., Optimization of SABRE for polarization of the tuberculosis drugs pyrazinamide and isoniazid. J. Magn. Reson. **2013,** 237, 73-78; (d) Shchepin, R. V.; Jaigirdar, L.; Chekmenev, E. Y., Spin–Lattice Relaxation of Hyperpolarized Metronidazole in Signal Amplification by Reversible Exchange in Micro-Tesla Fields. The Journal of Physical Chemistry C **2018,** 122 (9), 4984-4996.

14. (a) Manoharan, A.; Rayner, P. J.; Fekete, M.; Iali, W.; Norcott, P.; Hugh Perry, V.; Duckett, S. B., Catalyst-Substrate Effects on Biocompatible SABRE Hyperpolarization. **2019,** 20 (2), 285-294; (b) Shi, F.; Coffey, A. M.; Waddell, K. W.; Chekmenev, E. Y.; Goodson, B. M., Nanoscale Catalysts for NMR Signal Enhancement by Reversible Exchange. The Journal of Physical Chemistry C **2015,** 119 (13), 7525-7533; (c) Nelson, S. J.; Kurhanewicz, J.; Vigneron, D. B.; Larson, P. E. Z.; Harzstark, A. L.; Ferrone, M.; van Criekinge, M.; Chang, J. W.; Bok, R.; Park, I.; Reed, G.; Carvajal, L.; Small, E. J.; Munster, P.; Weinberg, V. K.; Ardenkjaer-Larsen, J. H.; Chen, A. P.; Hurd, R. E.; Odegardstuen, L.-I.; Robb, F. J.; Tropp, J.; Murray, J. A., Metabolic Imaging of Patients with Prostate Cancer Using Hyperpolarized [1-¹³C]Pyruvate. Science Translational Medicine **2013,** 5 (198), 198ra108; (d) Tickner, B. J.; Iali, W.; Roy, S. S.; Whitwood, A. C.; Duckett, S. B., Iridium α-Carboxyimine Complexes Hyperpolarized with para-Hydrogen Exist in Nuclear Singlet States before Conversion into Iridium Carbonates. ChemPhysChem **2019,** 20 (2), 241-245.

15. Appleby, K. M.; Mewis, R. E.; Olaru, A. M.; Green, G. G. R.; Fairlamb, I. J. S.; Duckett, S. B., Investigating pyridazine and phthalazine exchange in a series of iridium complexes in order to define their role in the catalytic transfer of magnetisation from parahydrogen. Chem. Sci. **2015,** 6 (7), 3981-3993.

16. (a) Eshuis, N.; Hermkens, N.; van Weerdenburg, B. J. A.; Feiters, M. C.; Rutjes, F. P. J. T.; Wijmenga, S. S.; Tessari, M., Toward nanomolar detection by NMR through SABRE hyperpolarization. J. Am. Chem. Soc. **2014,** 136 (7), 2695-2698; (b) Fekete, M.; Bayfield, O. W.; Bayfield, O.; Duckett, S. B.; Hart, S.; Mewis, R. E.; Pridmore, N.; Rayner, P. J.; Whitwood, A., Iridium(III) hydrido N-heterocyclic carbene-phosphine complexes as catalysts in magnetization transfer reactions. Inorg. Chem. **2013,** 52 (23), 13453-13461; (c) van Weerdenburg, B. J. A.; Gloggler, S.; Eshuis, N.; Engwerda, A. H. J.; Smits, J. M. M.; de Gelder, R.; Appelt, S.; Wymenga, S. S.; Tessari, M.; Feiters, M. C.; Blumich, B.; Rutjes, F. P. J. T., Ligand effects of NHC-iridium catalysts for signal amplification by reversible exchange (SABRE). Chem. Commun. **2013,** 49 (67), 7388-7390; (d) Ellames, G. J.; Gibson, J. S.; Herbert, J. M.; McNeill, A. H., The scope and limitations of deuteration mediated by Crabtree's catalyst. Tetrahedron **2001,** 57 (46), 9487-9497; (e) Barskiy, D. A.; Kovtunov, K. V.; Koptyug, I. V.; He, P.; Groome, K. A.; Best, Q. A.; Shi, F.; Goodson, B. M.; Shchepin, R. V.; Coffey, A. M.; Waddell, K. W.; Chekmenev, E. Y., The Feasibility of Formation and Kinetics of NMR Signal Amplification by Reversible Exchange (SABRE) at High Magnetic Field (9.4 T). J. Am. Chem. Soc. **2014,** 136 (9), 3322-3325.

17. Tom, B. A.; Bhasker, S.; Miyamoto, Y.; Momose, T.; McCall, B. J., Producing and quantifying enriched para-H2. Rev. Sci. Instrum. **2009,** 80 (1), 016108.

18. Blight, A. R., Treatment of walking impairment in multiple sclerosis with dalfampridine. Therapeutic Advances in Neurological Disorders **2011,** 4 (2), 99-109.

19. Crabtree, R., Iridium compounds in catalysis. Accounts of Chemical Research **1979,** 12 (9), 331-337.

20. (a) Truong, M. L.; Shi, F.; He, P.; Yuan, B.; Plunkett, K. N.; Coffey, A. M.; Shchepin, R. V.; Barskiy, D. A.; Kovtunov, K. V.; Koptyug, I. V.; Waddell, K. W.; Goodson, B. M.; Chekmenev, E. Y., Irreversible catalyst activation enables hyperpolarization and water solubility for NMR signal amplification by reversible exchange. J. Phys. Chem. B **2014,** 118 (48), 13882-13889; (b) Cowley, M. J.; Adams, R. W.; Atkinson, K. D.; Cockett, M. C. R.; Duckett, S. B.; Green, G. G. R.; Lohman, J. A. B.; Kerssebaum, R.; Kilgour, D.; Mewis, R. E., Iridium N-heterocyclic carbene complexes as efficient catalysts for magnetization transfer from para-hydrogen. J. Am. Chem. Soc. **2011,** 133 (16), 6134-6137.

21. (a) Golman, K.; Ardenkjær-Larsen, J. H.; Petersson, J. S.; Månsson, S.; Leunbach, I., Molecular imaging with endogenous substances. Proceedings of the National Academy of Sciences **2003,** 100 (18), 10435; (b) Kaptein, R.; Dijkstra, K.; Tarr, C. E., A Single-Scan Fourier Transform Method for Measuring Spin-Lattice Relaxation Times. J. Magn. Reson. **1976,** 24 (2), 295-300.

22. Rayner, P. J.; Burns, M. J.; Olaru, A. M.; Norcott, P.; Fekete, M.; Green, G. G. R.; Highton, L. A. R.; Mewis, R. E.; Duckett, S. B., Delivering strong (1)H nuclear hyperpolarization levels and long magnetic lifetimes through signal amplification by reversible exchange. PNAS **2017,** 114 (16), E3188-E3194.

23. (a) Green, R. A.; Adams, R. W.; Duckett, S. B.; Mewis, R. E.; Williamson, D. C.; Green, G. G. R., The theory and practice of hyperpolarization in magnetic resonance using parahydrogen. Prog. Nucl. Magn. Reson. Spectrosc. **2012,** 67, 1-48; (b) Eshuis, N.; Aspers, R. L. E. G.; van Weerdenburg, B. J. A.; Feiters, M. C.; Rutjes, F. P. J. T.; Wijmenga, S. S.; Tessari, M., Determination of long-range scalar 1H–1H coupling constants responsible for polarization transfer in SABRE. J. Magn. Reson. **2016,** 265, 59-66.

24. (a) Kumar, D.; Krishnan, Y.; Paranjothy, M.; Pal, S., Analysis of Molecular Interaction of Drugs within β-Cyclodextrin Cavity by Solution-State NMR Relaxation. The Journal of Physical Chemistry B **2017,** 121 (13), 2864-2872; (b) Kim, J.; Liu, M.; Hilty, C., Modeling of Polarization Transfer Kinetics in Protein Hydration Using Hyperpolarized Water. The Journal of Physical Chemistry B **2017,** 121 (27), 6492-6498; (c) Fairhurst, D.; Cosgrove, T.; Prescott, S. W., Relaxation NMR as a tool to study the dispersion and formulation behavior of nanostructured carbon materials. Magnetic Resonance in Chemistry **2016,** 54 (6), 521-526; (d) Grant, D. M.; Mayne, C. L.; Liu, F.; Xiang, T. X., Spin-lattice relaxation of coupled nuclear spins with applications to molecular motion in liquids. Chem. Rev. (Washington, DC, U. S.) **1991,** 91 (7), 1591-1624.

25. Mewis, R. E.; Fekete, M.; Green, G. G. R.; Whitwood, A. C.; Duckett, S. B., Deactivation of signal amplification by reversible exchange catalysis, progress towards in vivo application. Chem. Commun. **2015,** 51 (48), 9857-9859.

26. Taglang, C.; Korenchan, D. E.; von Morze, C.; Yu, J.; Najac, C.; Wang, S.; Blecha, J. E.; Subramaniam, S.; Bok, R.; Van-Brocklin, H. F.; Vigneron, D. B.; Ronen, S. M.; Sriram, R.; Kurhanewicz, J.; Wilson, D. M.; Flavell, R. R., Late-stage deuteration of 13C-enriched substrates for T1 prolongation in hyperpolarized 13C MRI. Chem. Commun. **2018,** 54 (41), 5233-5236.

27. (a) Busacca, C. A.; Fandrick, D. R.; Song, J. J.; Senanayake, C. H., The Growing Impact of Catalysis in the Pharmaceutical Industry. Adv. Synth. Catal. **2011,** 353 (11-12), 1825-1864; (b) Thompson, D. T., Some basic research in coordination chemistry and catalysis, related to applications for industry. Coordination Chemistry Reviews **1996,** 154, 179-192.

28. Hovener, J. B.; Schwaderlapp, N.; Borowiak, R.; Lickert, T.; Duckett, S. B.; Mewis, R. E.; Adams, R. W.; Burns, M. J.; Highton, L. A. R.; Green, G. G. R.; Olaru, A.; Hennig, J.; von Elverfeldtt, D., Toward Biocompatible Nuclear Hyperpolarization Using Signal Amplification by Reversible Exchange: Quantitative in Situ Spectroscopy and High-Field Imaging. Anal. Chem. **2014,** 86 (3), 1767-1774.

Supporting Information

Reaction monitoring using SABRE-hyperpolarized benchtop (1 T) NMR spectroscopy

Olga Semenova,[a] Peter M. Richardson,[a] Andrew J. Parrott,[b] Alison Nordon,[b] Meghan E. Halse [*a] and Simon B. Duckett [*a]

a Centre for Hyperpolarisation in Magnetic Resonance, Chemistry, The University of York, York, YO10 5NY, UK.

b WestCHEM, Department of Pure and Applied Chemistry and CPACT, University of Strathclyde, Glasgow, G11XQ, UK

Meghan Halse meghan.halse@york.ac.uk

Simon Duckett simon.duckett@york.ac.uk

Contents

Quantification of substrate to catalyst ratios and the level of deuterium incorporation

The substrate to catalyst ratio was calculated from the ratio between the integrals of the peaks associated with appropriate proton resonances of the free substrate and the catalyst. In the cases where a mixture of iridium catalyst species were detected, the substrate integral was referenced to the sum of the proton resonances responsible for the same proton sites for the different bound forms of the substrate in the catalyst.

The deuteration percentage was calculated using Equation S1, where S_{ortho} and S_{meta} are the integrated signal intensities for the *ortho* and *meta* resonances of the free substrate, respectively. In all cases, sufficient time was left between observations to allow for relaxation and accurate integration.

$$D\ (\%) = 100 * (1 - \frac{S_{ortho}}{S_{meta}}) \qquad \text{(Eq. S1)}$$

Evidence of the 4-aminopyridine (**4-AP**) *ortho* position deuteration

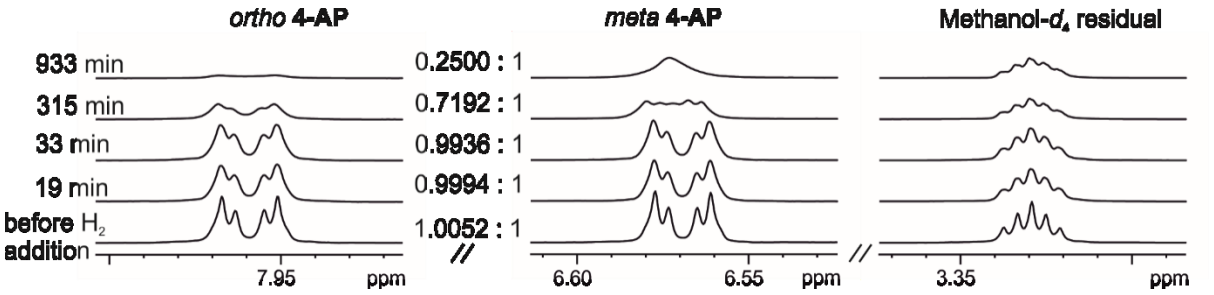

Figure S1 – Change in the relative integrals and line-shapes of the *ortho* and *meta* proton resonances of **4-AP** as a function of reaction time in the regime where H_2 (4 bar absolute) was added once at the beginning of the experiment. Time zero denotes the time at which the H_2 gas was first introduced to the sample. The line-shape of the *ortho* resonance is relatively unchanged with time; however, the line-shape of the *meta* resonance tends to a singlet over the course of the experiment. This change in line-shape is indicative of the substitution of ^1H for ^2H in the adjacent *ortho* position.

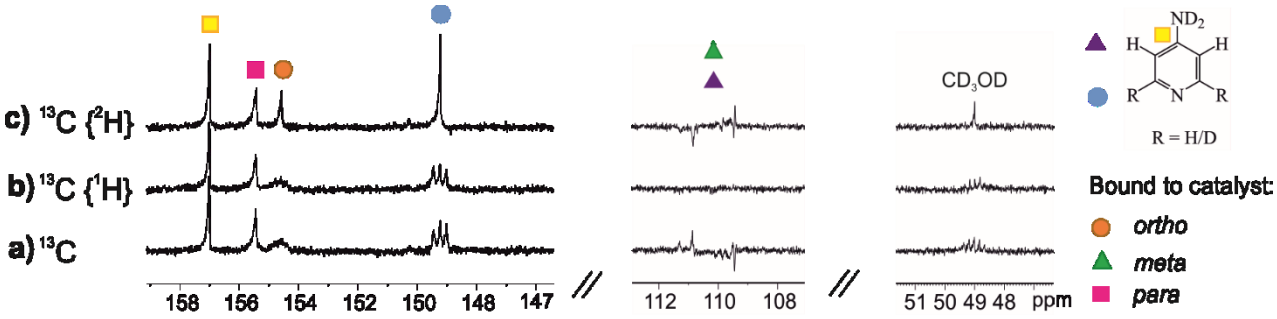

Figure S2 – ^{13}C NMR SABRE signals from a partially deuterated sample of 4-aminopyridine (5 eq, **4-AP**) in the presence of activated catalyst $[Ir(H)_2(IMes)(\mathbf{4\text{-}AP})_3]Cl$ (**4**) in MeOD under 4 bar *p*-H_2. The *ortho* carbon signal of free (blue circle) and bound (orange circle) **4-AP** shows splitting from deuterium (J^{CD} = 26.6 Hz) in both the ^{13}C and $^{13}C\{^1H\}$ SABRE NMR spectra. This splitting is removed in the $^{13}C\{^2H\}$ SABRE NMR spectrum. This confirms its origin from deuteration of the *ortho* position. The resonance for the *meta* carbon (purple and green triangles) signal appears in antiphase and consequently vanishes on proton decoupling in the corresponding $^{13}C\{^1H\}$ SABRE NMR spectrum; there is minimal change when a $^{13}C\{^2H\}$ SABRE NMR spectrum is recorded.

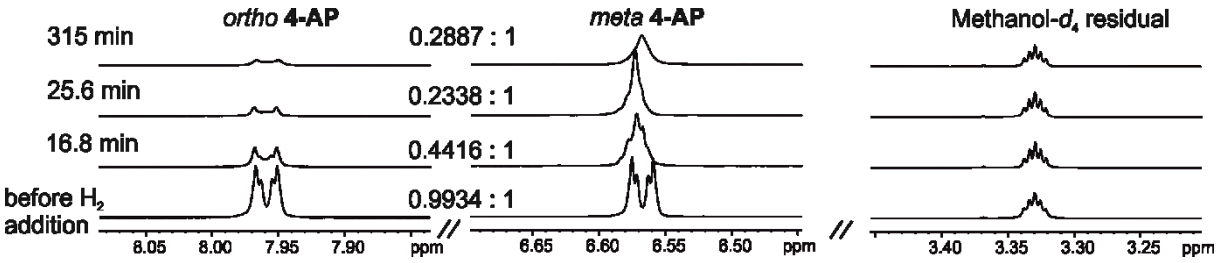

Figure S3 – Change in the relative intensity and line-shape of the *ortho* and *meta* proton resonances of **4-AP** as a function of reaction time in the regime where the *p*-H_2 was refreshed between each scan. Analogous to Figure S1, the *ortho* resonance line shape loses some of the second order splitting, which is characteristic of progressive ^2H substitution at the second *ortho* position on the ring, but retains the doublet line-shape indicating that the *meta* resonance itself is not undergoing deuteration. The line-shape of the *meta* resonance evolves into a singlet over time which suggests that the *ortho* position has been significantly deuterated. We note that the line-shape of the *meta* resonance indicates that significant incorporation of deuterium in the *ortho* position has occurred after only 25.6 min under these reaction conditions (see Fig. S4). Time zero denotes the time at which the H_2 gas was introduced to the sample.

Standard ^1H NMR reaction monitoring of the SABRE catalyst activation with 4-aminopyridine (**4-AP**) and 4-methylpyridine (**4-MP**)

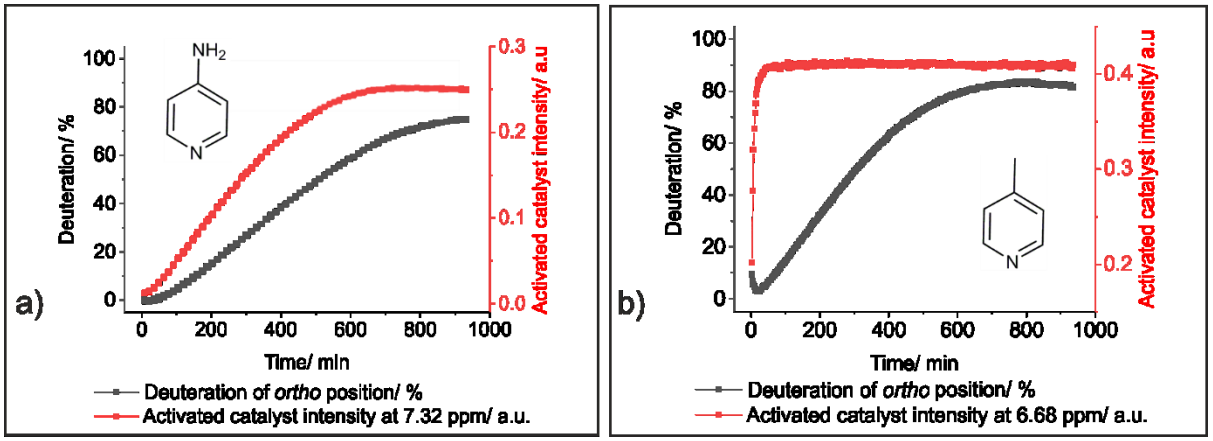

Figure S4 – In red: formation of the activated catalyst $[Ir(H)_2(IMes)(substrate)_3]Cl$ with **4-AP** (a) and **4-MP** (b) (both contain 25 mM of substrate and 5 mM of the pre-catalyst **1** in the starting solution) in methanol-d_4 under hydrogen gas (4 bar absolute). In black: deuteration level for the *ortho* position of the substrate **4-AP** during the catalyst activation. The deuteration curve for **4-MP** shows an initial fall that is not real, but instead reflects a decrease in the free *meta* peak integral due to partial overlap with a pre-catalyst resonance, a change in line-broadening also contributes to this.

Reaction monitoring with SABRE signal

A series of SABRE hyperpolarization experiments were performed using a 400 MHz ^{1}H NMR spectrometer for detection. Fresh *para*hydrogen was added to the head-space of the NMR tube and mixed into solution (via shaking) between each measurement to achieve SABRE hyperpolarization. This hydrogen refreshment step will change the observed rate of reaction for both the activation and the deuteration processes. To establish a suitable control experiment, a thermal ^{1}H NMR spectrum was recorded at each step of the experiment for comparison with the SABRE response. The evolution of the standard and SABRE-enhanced ^{1}H NMR signal intensities as a function of time, where *p*-H_2 is refreshed between each data point, is presented in Figure S5a and S5b,c, respectively. Here we use the *meta* proton resonance of **4-AP** in free solution (δ 6.58 ppm) as the probe because no deuteration of this position is observed on the timescale of our experiments.

An exponential fit of the standard ^{1}H NMR response (Figure S5a) indicates that the activation process was complete after 235 min. As expected, the SABRE-enhanced NMR response increases on the same timescale due to the increased concentration of the active SABRE catalyst (**4**). Interestingly, the SABRE signal continues to grow after the activation is complete. These results suggest that the SABRE-enhanced NMR signal is affected by both the activation and deuteration processes. However, differentiation of these effects is challenging (see paper). Similar trends were observed at both 9.4 T (Figure S5b) and 1 T (Figure S5c).

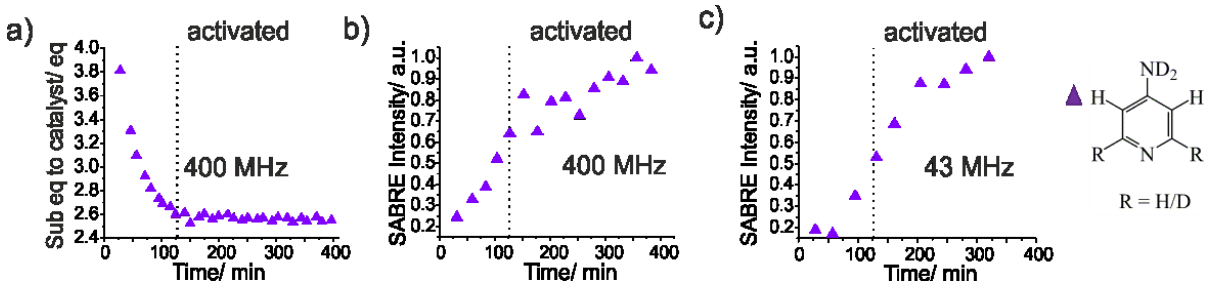

Figure S5 – (a) Ratio of free substrate to catalyst as a function of reaction time, determined from standard ^{1}H NMR spectra acquired at 9.4 T in parallel with the SABRE measurements. The time to activation (235 min) was determined from a fit to a mono-exponential decay. Normalised raw SABRE-enhanced ^{1}H NMR signal intensity of the *meta* proton of **4-AP** (5 eq relatively to **1**) during the activation of SABRE complex in methanol-d_4 as measured using detection at (b) 9.4 T and (c) 1 T.

Variable flip angle single-shot sequence for relaxation time measurement

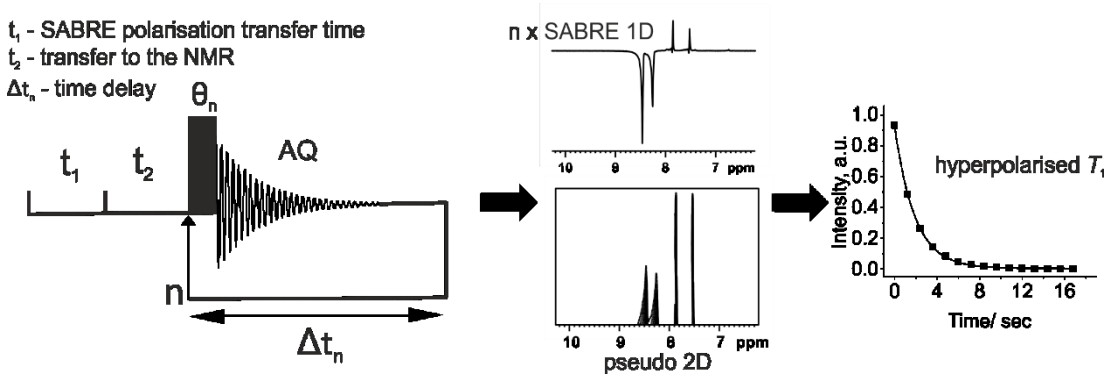

Figure S6 – Schematic representation of a single-shot hyperpolarized T_1 measurement with a small flip angle sequence.

In the variable flip angle pulse sequence illustrated in Figure S6 a series of *N* FIDs is recorded where each FID is associated with an RF pulse with a unique flip angle, θ_n. $M_{xy,n}$ and $M_{z,n}$ are defined as the amplitude of the transverse and longitudinal magnetization vectors immediately following the *n*th RF pulse, respectively. The time between RF pulses is Δt_n, where the subscript *n* denotes the delay between θ_n and θ_{n+1} and $\Delta t_0 = 0$ by definition. The initial magnetization along the *z* axis prior to the first RF pulse, M_0, is the initial amplitude of the hyperpolarization. If we consider only the decay of this hyperpolarization, i.e. neglecting the build-up of any thermal magnetization, we can write the following recurrence relationships to describe the amplitude of the transverse and longitudinal components of the magnetization following the *n*th RF pulse, where T_1 is the hyperpolarization lifetime and $M_{z,0} = M_0$:

$$M_{xy,n} = M_{z,n-1}\exp(-\Delta t_{n-1}/T_1)\sin\theta_n \qquad \text{(S2)}$$

$$M_{z,n} = M_{z,n-1}\exp(-\Delta t_{n-1}/T_1)\cos\theta_n \qquad \text{(S3)}$$

To directly monitor the decay of the magnetization with an optimal signal-to-noise ratio, we choose the variable flip angles according to the following two constraints:

(1) In the absence of T_1 relaxation, the amount of transverse magnetization resulting from each RF pulse is the same for all *N* RF pulses.

(2) As much of the magnetization along *z* is sampled during the experiment as possible. Therefore the angles are chosen such that $M_{z,N} \to 0$ while not violating condition (1).

In the absence of T_1 relaxation, Eqs. S2 and S3 simplify to Eqs. S4 and S5 and we define the tangent of the flip angle, θ_n, in terms of the ratio of the transverse and longitudinal magnetization (Eq. S6).

$$M_{xy,n} = M_{z,n-1}\sin\theta_n \qquad \text{(S4)}$$

$$M_{z,n} = M_{z,n-1}\cos\theta_n \qquad \text{(S5)}$$

$$\tan\theta_n = \frac{M_{xy,n}}{M_{z,n}} \qquad \text{(S6)}$$

Substituting Eq. S6 into Eq. S4, we obtain the following:

$$\frac{M_{xy,n}}{M_{xy,n-1}} = \frac{\sin\theta_n}{\tan\theta_{n-1}} \qquad \text{(S7)}$$

To fulfil condition (1), $M_{xy,n} = M_{xy,n-1}$ for all *n* in the absence of T_1 relaxation. Therefore Eq. S7 simplifies to Eq. S8, which is defined for all *N* flip angles as long as $|\theta_{N-1}| \leq \frac{\pi}{4}$.

$$\sin\theta_n = \tan\theta_{n-1} \qquad \text{(S8)}$$

Condition (2) is met by determining the maximum value of θ_1 for which $|\theta_{N-1}| \leq \frac{\pi}{4}$. Table S1 presents the set of angles that fulfil conditions (1) and (2) where *N* = 15. In the absence of T_1 relaxation, 25.6% of the initial hyperpolarization, M_0, is excited by each of the 15 variable flip angles.

In the presence of relaxation, the transverse magnetization created by each RF pulse is given by Eq. S9.

$$M_{xy,n} = M_{z,n-1}\exp(-\Delta t_{n-1}/T_1)\tan\theta_{n-1} \qquad \text{(S9)}$$

Substituting in Eq. S6, we get the following recurrence relationship for the transverse magnetization:

$$M_{xy,n} = M_{xy,n-1}\exp(-\Delta t_{n-1}/T_1) = M_0\sin\theta_1\exp(-t_n/T_1) \qquad \text{(S10)}$$

where $t_n$is defined in Eq. S11.

$$t_n = \sum_{m=1}^{n-1}\Delta t_m \qquad \text{(S11)}$$

Therefore, the signal observed using the variable flip angle sequence will have an initial amplitude of $M_0\sin\theta_1$ and will decay according to the hyperpolarization lifetime. It is important to note that this analysis does not model the effects of the variable flip angle pulse sequence on the recovery of the thermal magnetization during the experiment. These effects are removed by performing a reference measurement without hyperpolarization (see Figure S7), as described in the main text.

Table S1 – Variable flip angles and corresponding z-magnetisation and xy-magnetisation levels (%) for an optimised variable flip angle sequence with N = 15.

Experiment number	**Flip angle / degrees**	**M_z / %**	**M_{xy} /%**
1	15.0	96.6%	25.9%
2	15.5	93.1%	25.8%
3	16.1	89.4%	25.8%
4	16.8	85.6%	25.8%
5	17.5	81.6%	25.7%
6	18.4	77.5%	25.8%
7	19.5	73.0%	25.9%
8	20.7	68.3%	25.8%
9	22.2	63.3%	25.8%
10	24.1	57.7%	25.8%
11	26.6	51.6%	25.9%
12	30.0	44.7%	25.8%
13	35.2	36.5%	25.8%
14	44.9	25.9%	25.8%
15	86.2	1.7%	25.8%

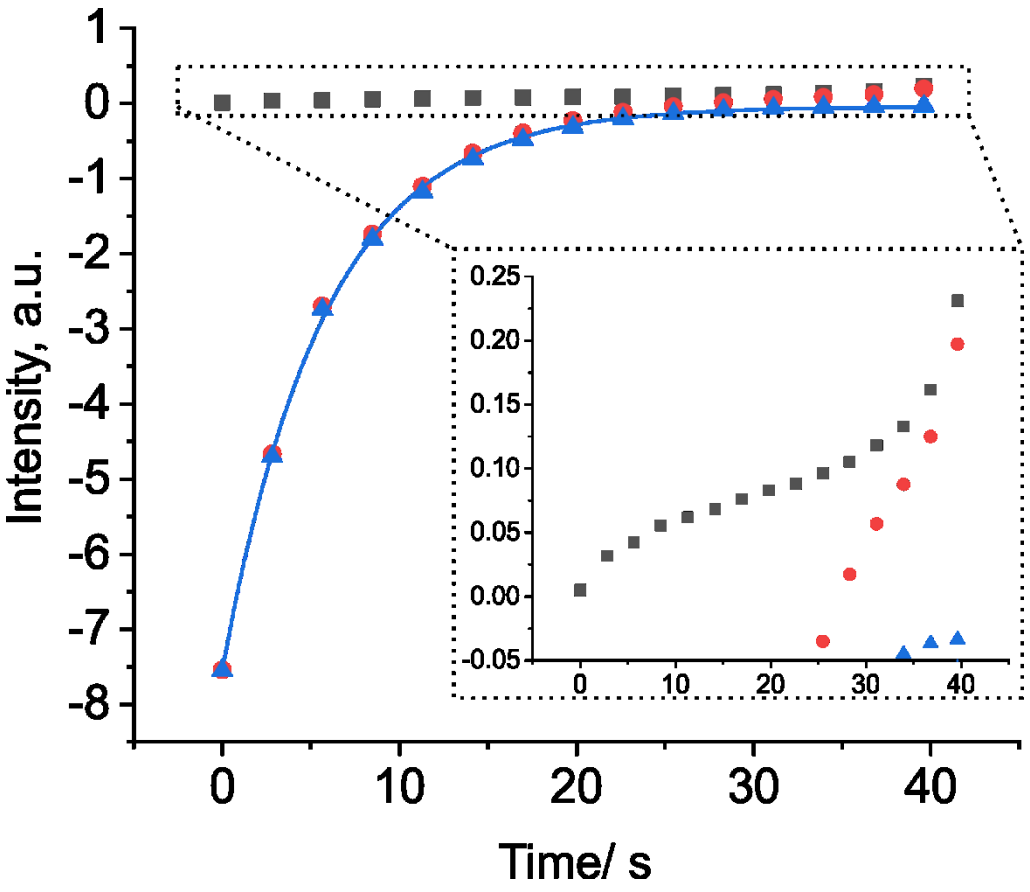

Figure S7 – The evolution of the hyperpolarized and thermal magnetisation in an example variable flip angle single-shot measurement for free 4-methylpyridine (**4-MP**) *ortho* proton (8.39 ppm) in the presence of $[Ir(H)_2(IMes)(\mathbf{4\text{-}MP})_3]Cl$ in methanol-d_4 at 298 K. The relaxation of the hyperpolarized signal with time is presented in red circles. Thermal polarization build-up measured in the reference scan is shown in grey squares. The resultant corrected hyperpolarization decay curve (the difference between the hyperpolarized and thermal reference measurements) is presented in blue triangles. Inset is a zoomed region of the graph illustrating the thermal polarization increase with time in the reference scan.

Figure S8 presents a comparison of the variable flip angle pulse sequence (red) and a comparable measurement using a constant flip angle sequence with $\theta = 5°$ (black). While the measured relaxation time is the same for both sequences, the use of the variable flip angle sequence improves the SNR by more than a factor of 3 and hence the accuracy of the final T_1.

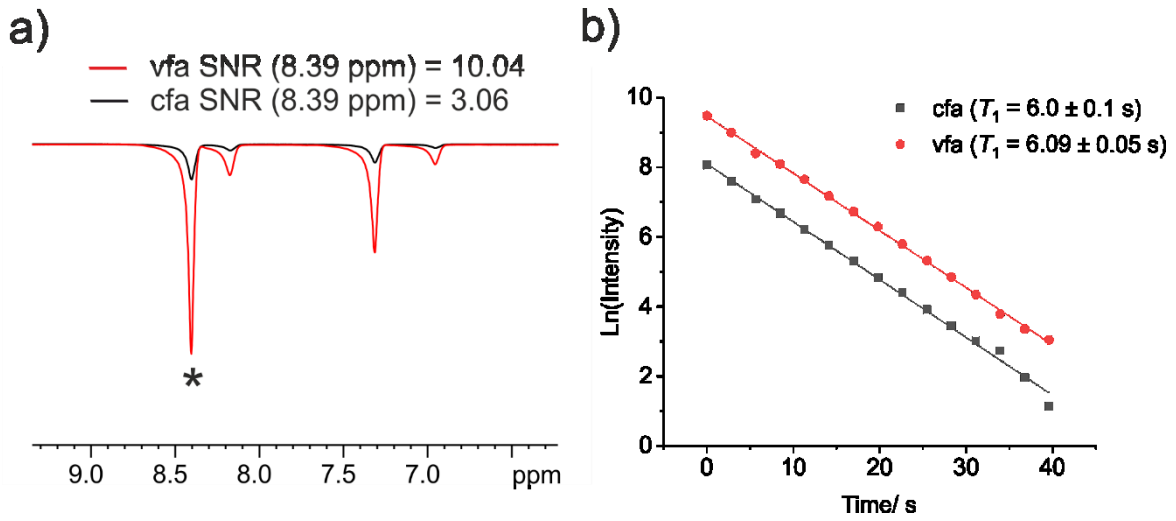

Figure S8 – a) First spectrum from hyperpolarized variable (vfa, red) and constant (cfa, black) flip angle sequences for free 4-methylpyridine (**4-MP**) in the presence of $[Ir(H)_2(IMes)(\mathbf{4\text{-}MP})_3]Cl$ in methanol-d_4 at 298 K. b) Relaxation curves for the resonance at 8.39 ppm (*ortho* protons of free **4-MP**) of the same sample on a logarithmic scale acquired with hyperpolarized variable (red) and constant (black) flip angle sequences.

The standard error for 5 repeated variable flip angle single-shot T_1 measurements was less than 3% for the samples of 25 mM **4-AP** in MeOH in the presence of the 1 mM, 2 mM, 3 mM and 4 mM activated SABRE catalyst and less than 6% for the samples of 25 mM **4-AP** in MeOH in the presence of the 0.5 mM and 5 mM activated SABRE catalyst measured on the 1 T benchtop NMR spectrometer.

Activation monitoring with 4-methylpyridine using hyperpolarization lifetimes

The formation of the SABRE catalyst $[Ir(H)_2(IMes)(\mathbf{4\text{-}MP})_3]Cl$ in the mixture of **1** and $[Ir(COD)(IMes)(\mathbf{4\text{-}MP})]Cl$ in the presence of a 4-fold excess (in starting solution) of 4-methylpyridine (**4-MP**) was monitored using the hyperpolarization lifetime measurement procedure with benchtop (1 T) NMR detection. Figure S9 shows the change in the *ortho* (green square) and *meta* (gold triangles) ^1H hyperpolarization lifetimes of **4-MP** as a function of reaction time after the initial addition of *p*-H_2 in methanol-d_4 (Figure S9a) and *protio* methanol (Figure S9b). Figure S9 indicates a much faster rate of activation for **4-MP** compared to **4-AP** (Figure 3 in main text). This is due to the different electronic properties of **4-MP** and **4-AP**. Furthermore, the hyperpolarization lifetime behaviour for **4-MP** is the same in the two solvents. This indicates that there is no significant deuteration of **4-MP** on the timescale of this experiment. Control experiments of ^1H NMR line-shapes were acquired at 400 MHz to confirm the absence of significant deuteration on this timescale in the regime when *p*-H_2 is refreshed between the measurements (see Figure S10).

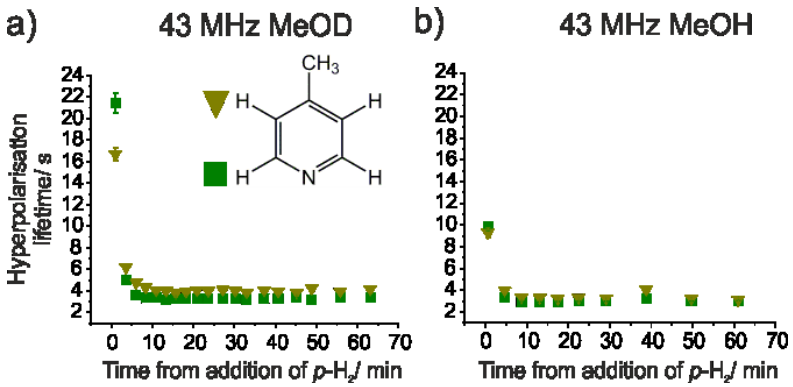

Figure S9 – Hyperpolarization lifetimes of the *ortho* and *meta* protons of **4-MP** as a function of time during the activation of the SABRE complex at 1 T (a) in methanol-d_4 and (b) in *protio* methanol. Initial concentration of **4-MP** is 25 mM which results in a 2-fold excess to the activated complex $[Ir(H)_2(IMes)(\mathbf{4\text{-}MP})_3]Cl$ (5 mM). Error bars represent the standard error from the fit of each hyperpolarization decay curve to equation 1 in the main text.

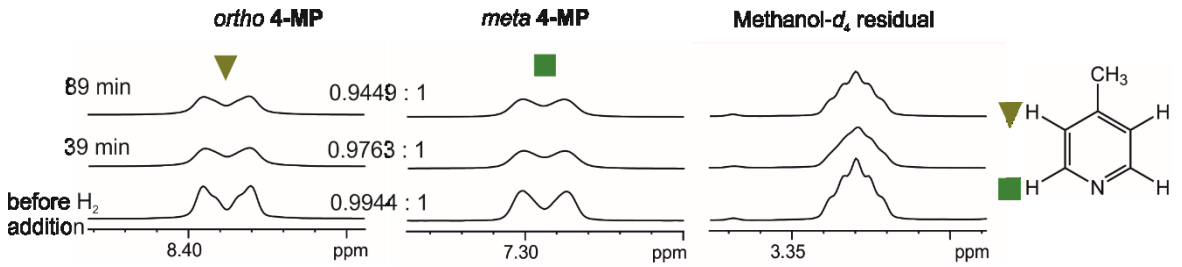

Figure S10 – Change in the relative intensity of the **4-MP** *ortho* and *meta* resonances as a function of reaction time in the regime when the *p*-H_2 was refreshed between each scan acquired at 400 MHz. The initial solution was prepared with 9 eq of **4-MP** relative to **1**. Eleven *p*-H_2 refreshments were completed over 89 min. The ^1H NMR spectra presented were acquired (bottom) before *p*-H_2 addition, (middle) 39 min and (top) 89 min after the first *p*-H_2 addition. No significant change was observed in the line-shape of the *ortho* and *meta* peaks of **4-MP**, indicating that no significant deuteration occurs on this timescale. Time zero denotes the time at which the *p*-H_2 gas was introduced into the sample.

Characterisation

4-aminopyridine (4-AP)

^{1}H (400.1 MHz, MeOD, 253 K, ppm): 7.94 (m, 2H, *ortho*H), 6.55 (m, 2H, *meta*H).

^{13}C (100.6 MHz, MeOD, 253 K, ppm): 156.8 (C), 149.1 (*ortho*CH), 109.7 (*meta*CH).

^{15}N (50.7 MHz, MeOD, 243 K, ppm): 254.1 (N), 66.0 (NH_2).

[Ir(COD)(IMes)(4-aminopyridine)]Cl (2) (also [Ir(COD)(IMes)(4-AP)]Cl)

^{1}H (500.1 MHz, MeOD, 253 K): 7.40 (s, 2H, NCHCHN), 7.21 (s, 2H, CH^{mes}), 7.13 (m, 2H, *ortho*H, 4-AP *trans* to COD), 7.05(s, 2H, CH^{mes}), 6.32 (m, 2H, *meta*H, 4-AP *trans* to COD), 3.52 (m, 2H, CH^{COD}), 3.33 (overlap with solvent, CH^{COD}), 2.44 (s, 6H, *para*CH_3^{mes}), 2.34 (br s, 6H, *ortho*CH_3^{mes}), 1.94 (s, 6H, *ortho*CH_3^{mes}), 1.98 and 1.86 and 1.59 (br m, 8H, overlap, CH_2^{COD})**.**

^{13}C (125.8 MHz, MeOD, 253 K): 174.2 (NCN), 155.1 (*para*C, 4-AP), 149.1 (*ortho*CH, 4-AP), 139.5 (*para*C^{mes}), 137.4 (N-C^{mes}), 135.4 (*ortho*C^{mes}), 135.2 (*ortho*C^{mes}), 129.5 (CH^{mes}), 129.0 (CH^{mes}), 125.0 (NCHCHN), 109.7 (*meta*CH, 4-AP), 80.8 (CH^{COD}), 62.7 (CH^{COD}), 19.8 (*para*CH_3^{mes}), 17.4 (*ortho*CH_3^{mes}), 32.3 (overlap, CH_2^{COD}), 29.06 (overlap, CH_2^{COD})**.**

^{15}N (50.7 MHz, MeOD, 243 K): 195.6 (aromatic N, 4-AP), 195.0 (carbene N), 72.1 (NH_2, 4-AP).

[Ir(H)$_2$(IMes)(4-aminopyridine)$_3$]Cl (4) (also [Ir(H)$_2$(IMes)(4-AP)$_3$]Cl)

^{1}H NMR (400.1 MHz, MeOD, 253 K): 7.65 (m, 4H, *ortho*H, 4-AP *trans* to hydride), 7.37 (m, 2H, *ortho*H, 4-AP *cis* to hydride), 7.01 (s, 2H, NCHCHN), 6.75 (s, 4H, CH^{mes}), 6.15 (m, 4H, *meta*H, 4-AP *trans* to hydride), 6.04 (m, 2H, *meta*H, 4-AP *cis* to hydride), 2.26 (s, 6H, *p*CH_3^{mes}), 2.05 (s, 12 H, *o*CH_3^{mes}), −22.97 (s, 2H, hydride).

^{13}C NMR (100.6 MHz, MeOD, 253 K): 155.93 (NCN), 155.26 (*ortho*C, 4-AP cis to hydride), 155.11 (*para*C, 4-AP cis to hydride), 155.08 (*para*C, 4-AP trans to hydride), 154.44 (*ortho*C, 4-AP trans to hydride), 139.27 (*ortho*C^{mes}), 138.96 (*para*C^{mes}), 136.14 (N-C^{mes}), 129.28 (CH^{mes}), 122.95 (NCHCHN), 110.0 (*meta*C, 4-AP trans to hydride), 109.77 (*meta*C, 4-AP cis to hydride), 20.92 (*para*CH_3^{mes}), 18.90 (*ortho*CH_3^{mes}).

^{15}N (50.7 MHz, MeOD, 253 K): 214.10 (N, 4-AP *trans* to hydride), 196.90 (N, 4-AP *cis* to hydride), 194.00 (carbene N), 67.29 (NH_2, 4-AP *cis* to hydride, at 243 K), 66.35 (NH_2, 4-AP *trans* to hydride, at 243 K).

4-methylpyridine (4-MP)

^{1}H (500.1 MHz, MeOD, 263 K): 8.40 (m, 2H, *ortho*H), 7.34 (m, 2H, *meta*H), 2.43 (s, 3H, CH_3).

^{13}C (125.8 MHz, MeOD, 263 K): 149.2 (C), 148.1 (*ortho*CH), 125.2 (*meta*CH), 19.6 (CH_3).

^{15}N (50.7 MHz, MeOD, 255 K): 188.7 (N, 4-MP).

[Ir(COD)(IMes)(4-methylpyridine)]Cl (also [Ir(COD)(IMes)(4-MP)]Cl)

^{1}H (500.1 MHz, MeOD, 263 K): 7.70 (overlap, 2H, *ortho*H, 4-MP *trans* to COD), 7.41 (s, 2H, NCHCHN), 7.24 (br s, 2H, CH^{mes}), 7.15 (m, 2H, *meta*H, 4-MP *trans* to COD), 7.02 (br s, 2H, CH^{mes}), 3.66 (t, 2H, J^{HH} = 2.8 Hz, CH^{COD}, *trans* to 4-MP), 3.28 (t, 2H, J^{HH} = 2.8 Hz, CH^{COD}, *trans* to carbene), 2.46 (s, 6H,

paraCH_3^{mes}), 2.43 (s, 3H, CH_3, 4-MP *trans* to COD), 2.37 (br s, 6H, *ortho*CH_3^{mes}), 1.86 (br s, 6H, *ortho*CH_3^{mes}), 2.05, 1.90, 1.65, 1.64 (overlap, CH_2^{COD}).

^{13}C (125.8 MHz, MeOD, 263 K): 173.0 (NCN), 150.1 (*para*C, 4-MP), 149.9 (*ortho*CH, 4-MP), 139.8 (*para*C^{mes}), 135.7 and 135.3 (*ortho*C^{mes}), 133.2 (N-C^{mes}), 129.1 (CH^{mes}), 126.5 (*meta*CH, 4-MP), 125.2 (NCHCHN), 81.8 (CH^{COD}, *trans* to carbene), 64.4 (CH^{COD}, *trans* to 4-MP), 19.8 (*para*CH_3^{mes}), 19.5 (CH_3, 4-MP), 17.3 (*ortho*CH_3^{mes}), 28.5 (overlap, CH_2^{COD}), 32.1 (overlap, CH_2^{COD}).

^{15}N (50.7 MHz, MeOD, 263 K): 233.5 (aromatic N, 4-MP), 195.4 (carbene N).

$[Ir(H)_2$(IMes)(4-methylpyridine)$_3]Cl$ (also $[Ir(H)_2$(IMes)(4-MP)$_3]Cl$)

^1H NMR (500.1 MHz, MeOD, 255 K): 8.15 (m, 4H, *ortho*H, 4-MP *trans* to hydride), 7.88 (m, 2H, *ortho*H, 4-MP *cis* to hydride), 7.11 (s, 2H, NCHCHN), 6.95 (m, 4H, *meta*H, 4MP *trans* to hydride), 6.82 (m, 2H, *meta*H, 4-MP *cis* to hydride), 6.67 (s, 4H, CH^{mes}), 2.34 (s, 6H, CH_3, 4-MP *trans* to hydride), 2.22 (s, 6H, *para*CH_3^{mes}), 2.16 (s, 3H, CH_3, 4-MP *cis* to hydride), 2.05 (s, 12H, *ortho*CH_3^{mes}), −22.64 (s, 2H, hydride).

^{13}C (125.8 MHz, MeOD, 255 K): 154.6 (*ortho*C, 4-MP cis to hydride), 153.6 (*ortho*C, 4-MP *trans* to hydride), 152.0 (NCN), 148.4 (*para*C, 4-MP *cis* to hydride), 148.0 (*para*C, 4-MP *trans* to hydride), 138.1 (*para*C^{mes}), 137.5 (N-C^{mes}), 135.1 (*ortho*C^{mes}), 128.3 (CH^{mes}), 122.54 (NCHCHN), 125.91-125.95 (overlap, *meta*C, 4-MP *trans* to hydride, *meta*C, 4-MP *cis* to hydride), 26.0 (CH_3, 4-MP *trans* to hydride, 4-MP *cis* to hydride), 19.7 (*para*CH_3^{mes}), 17.7 (*ortho*CH_3^{mes}).

^{15}N (50.7 MHz, MeOD, 255 K): 247.4 (N, 4-MP *trans* to hydride), 194.5 (carbene N), 130.8 (N, 4-MP *cis* to hydride).